Defect characterization studies on irradiated boron-doped silicon pad diodes and Low Gain Avalanche Detectors

Anja Himmerlich [a],[*], Nuria Castello-Mor [a], Esteban Currás Rivera [a], Yana Gurimskaya [a], Vendula Maulerova-Subert [a],[c], Michael Moll [a], Ioana Pintilie [b], Eckhart Fretwurst [c], Chuan Liao [c], Jörn Schwandt [c]

[a] European Organization for Nuclear Research, CERN, Esplanade des Particules 1, Geneva, 1211, Switzerland
[b] National Institute of Materials Physics, NIMP, Str. Atomistilor 105 bis, Bucharest, RO-77125, Romania
[c] Institute for Experimental Physics, University of Hamburg, Luruper Chaussee 149, Hamburg, 22761, Germany

ARTICLE INFO

ABSTRACT

High-energy physics detectors with internal charge multiplication, like Low Gain Avalanche Detectors (LGADs), that will be used for fast timing in the High Luminosity LHC experiments, have to exhibit a significant radiation tolerance. In this context, the impact of radiation on the highly boron-doped gain layer is of particular interest, since due to the so-called Acceptor Removal Effect (ARE) a radiation-induced deactivation of active boron dopants takes place, that is causing a progressive loss in the gain with increasing irradiation level. In this paper we present defect-spectroscopy measurements (Deep-Level Transient Spectroscopy and Thermally Stimulated Current technique) on neutron, proton and electron irradiated p-type silicon pad diodes of different resistivity as well as LGADs neutron irradiated at fluences up to 1×10^{15} n_{eq}/cm^2. We show that compared to silicon pad diodes the determination of LGAD defect introduction rates is less straightforward as they are strongly influenced by the impact of the gain layer. The measured gain layer capacitance has a strong frequency and temperature dependence which makes DLTS measurements challenging to perform with results difficult to interpret. With the TSC technique the defects formed in the LGADs are nicely observed and can be compared to the defects formed in the silicon pad diodes. However, the exact assignment of defects to the gain layer or bulk region remains challenging and the charge amplification effect of the LGADs impacts the exact determination of defect concentrations. We also demonstrate that, depending on the TSC measurement conditions, defect induced internal electric fields are built up in the irradiated LGADs which impact the signal current.

1. Introduction

Low Gain Avalanche Detectors (LGADs) are characterized by their high precision timing performance and are the selected technology for the ATLAS High-Granularity Timing Detector (HGTD) as well as the CMS Endcap timing layer (ETL) [1,2]. The operation of such sensors in the HL-LHC experiments requires a high radiation tolerance up to a 1 MeV neutron equivalent fluence Φ_{eq} of about 2×10^{16} n_{eq}/cm^2. The observed radiation induced degradation in the LGAD performance is associated with changes in the effective doping concentration N_{eff} of the highly doped gain layer [3]. Normally, the doping level in such a layer is up to 1×10^{17} cm^{-3} enabling charge multiplication due to impact ionization. The degradation becomes evident in a decrease in the signal gain with increasing particle fluence resulting in the disappearance of the charge multiplication at fluences of about 2×10^{15} n_{eq}/cm^2 [4].

The radiation-induced deactivation of boron as dopant in p-type silicon (Si) is a well-known process, called Acceptor Removal Effect

(ARE). Thereby, due to the interaction with high-energy particles, Si atoms are released from their lattice site and become Si interstitials (Si_i) which are very mobile, even at low temperatures, and interact via the Watkins replacement mechanism preferentially with boron and carbon atoms [5,6] forming boron and carbon interstitials (B_i, C_i). These interstitials can further interact and create boron and carbon related defects like e.g. B_iB_s, B_iO_i, B_iC_s, C_iC_s or C_iO_i, where "i" and "s" subscripts stand for interstitial and substitutional atom site in the crystal [7,8]. The interstitial boron–interstitial oxygen complex (B_iO_i) is generally considered as main responsible defect for the boron deactivation. Although recent publications also state a $B_{Si}Si_i$ as possible defect structure to explain the ARE [9], in this publication we will follow the so far widely accepted assumption of a B_iO_i defect structure. Its creation is coupled with the deactivation of one negatively charged boron atom B_s and the formation of a donor type defect with an energy level in the upper part of the Si band gap (E_C −0.25 eV). Accordingly,

---

Table 1

Samples overview: The samples were neutron irradiated according to the given fluences Φ_{eq}. For the LGADs the gain layer depletion voltages V_{GL} and for the PIN diodes the full depletion voltages V_{depl} are given in this table. The values were extracted from C–V measurements performed at −20 °C and with 10 kHz measurement frequency (our standard measurement conditions for irradiated LGADs). In brackets the values of the unirradiated sensors are added.

		Φ_{eq} (n_{eq}/cm^2)	V_{depl} (V)	V_{GL} (V)
LGAD (HPK)	W36 S3-L15P5	1×10^{13}	–	50.8 (51.2)
PIN (HPK)	W42 S4-L14P5	1×10^{13}	6.5 (7.2)	–
LGAD (CNM)	r11486 W2-U23	1×10^{14}	–	27.0 (39.0)
LGAD (CNM)	r11486 W3-A12	1×10^{14}	–	26.0 (30.5)
PIN (CNM)	r11486 W2-X22	1×10^{14}	0.6 (1.8)	–
LGAD (CNM)	r11486 W2-W22	1×10^{15}	–	14.0 (42.5)

the B_iO_i formation contributes with a factor of two to the changes of the space charge in the depletion region [8]. The formation of B_iO_i competes with the formation of C_iO_i which induces a hole trap at $E_V + 0.36\,eV$ and does not contribute to the ARE. This competition explains the improved radiation hardness of carbonated LGAD gain layers [4]. Summarized, the mentioned defect kinetic model described in detail in Ref. [8] assumes that all interstitials created during the radiation interaction are forming either B_iO_i or C_iO_i defects. This is very nicely reproduced in the experimentally observed dependency of B_iO_i introduction rates (IR = (defect concentration)/(fluence)) on the initial boron doping concentration for p-type silicon devices irradiated with fluences of up to $10^{15}\,n_{eq}/cm^2$. However, it seems not to be valid anymore for highly doped silicon, like the gain layers of LGADs, irradiated at fluences $> 10^{15}\,n_{eq}/cm^2$, since the generation rates reflecting deactivation of boron, extracted from the changes in the macroscopic properties of the device are much higher than expected from the defect kinetic model [4,8]. This raises the question if other defect structures might lead or contribute to the deactivation of acceptors in the highly doped LGAD gain layers. In order to trace back this question we present defect spectroscopy studies on silicon pad diodes and LGADs using the Deep-level Transient Spectroscopy (DLTS) and Thermally Stimulated Current (TSC) technique.

2. Materials and methods

The measurements were performed on LGADs and PIN diodes from CNM (Centro Nacional de Microelectrónica, Barcelona, Spain) and HPK (Hamamatsu Photonics, Japan). The LGAD structure is n^{++}–p^+–p–p^{++} with a thin highly boron-doped multiplication layer (p^+) of around 2 μm (this layer is missing in the PIN diodes), a low doped active bulk region of about 50 μm (p) as well as the highly doped electrodes (n^{++} and p^{++}). Irradiation was performed with reactor neutrons at the JSI in Ljubljana (Slovenia). The sample overview as well as the irradiation fluences are given in Table 1. The fluences given in this paper are normalized to 1 MeV neutron equivalent values (Φ_{eq}) using the non-ionizing energy loss scaling (NIEL). The LGADs from CNM are from run 11486 with an active area of $0.09\,cm^2$ and a physical thickness of 351 μm. They consist of a low resistivity p-type support wafer and a 50 μm boron-doped active layer with a resistivity of about 5 kΩcm into which, during the sensor processing, an active p-type multiplication layer is implanted underneath the front electrode. The HPK LGADs have an active area of $0.0169\,cm^2$ and consists of a 300 μm support wafer, a 50 μm active p-type layer and an active highly-boron doped p-type multiplication layer. After irradiation all samples were annealed for 10 min at 60 °C.

The defect spectroscopy measurements on the LGADs and PIN diodes are compared to similar studies performed on single boron-doped n^+–p–p^+ silicon pad diodes produced by CiS (Forschungsinstitut für Mikrosensorik GmbH, Erfurt, Germany) [10]. These diodes consist of an epitaxial grown boron-doped bulk layer of 50 μm that vary in resistivity from 10 Ωcm to 1 kΩcm. The active area of those devices is $6.927 \times 10^{-2}\,cm^2$. They were irradiated with reactor neutrons at JSI [11],

with 24 GeV/c protons at IRRAD proton facility (CERN) [12], with 230 MeV protons at Boston General Hospital (USA) or with 200 MeV electrons at CLEAR (CERN) [13], and annealed afterwards for 10 min at 60°C. As hardness factors for the Φ_{eq} calculation we used 0.62 for 23 GeV proton irradiation, 0.95 for 230 MeV proton irradiation and 0.082 for 200 MeV electron irradiation.

In order to investigate the macroscopic properties of the non-irradiated and irradiated diodes Capacitance–Voltage (C–V) measurements with different frequencies as well as Current–Voltage (I–V) measurements were performed. As defect spectroscopy methods Deep Level Transient Spectroscopy (DLTS) and Thermally Stimulated Current (TSC) were applied. For DLTS a commercial system from PhysTech GmbH [14] was used. Three time windows, of 20 ms, 200 ms and 2 s, were used for recording the capacitive transients following the carrier injection pulse during the temperature scan from 20 K to 280 K. To inject only majority carriers a pulse voltage of UP = −0.6 V was chosen, while for minority and majority carrier injection the pulse voltage was set to +2 V. The pulse duration (t_p) was varied between 0.1 ms and 100 ms. Before and after the injection pulse the device was put under reverse bias UR (typically UR = −10 V). The measurement frequency was 1 MHz.

TSC measurements were performed in the temperature range from 20 K to 220 K by using a Keithley electrometer and a Labview based DAQ. The typical measurement cycle for spectra presented in this paper consists of three steps:

(1) Cooling down: A reverse bias UR_{down} is applied to the diode at high temperature (≥ 220 K). Afterwards the biased diode is subsequently cooled down to a certain filling temperature T_{fill} (20 K to 90 K). This step assures that there is no charge trapped on the defects.

(2) Filling step: At T_{fill} a filling pulse UP (+20 V) is applied to the sensor for a specific filling time ($t_{fill} = 60\,s - 360\,s$). During this step the defect states are trapping majority and/or minority carriers.

(3) Heating up: The diode is put back under a reverse bias UR_{up} and the temperature is raised with a constant heating rate of $\beta = 11$ K/min, from T_{fill} to 220 K. During this step the current signal generated by thermal emission of carriers from the defect levels is recorded. In case that UR_{down} is equal to UR_{up} the reverse bias is just named UR in the following.

From the recorded TSC spectra the defect concentrations N_t were determined by integration over the measured TSC peaks using the following equation [15]:

$$N_t = 2 \frac{Q_t}{q_0 \cdot A \cdot d} = \frac{2}{q_0 \cdot A \cdot d \cdot \beta} \int I_{TSC}(T)\,dT \qquad (1)$$

with: Q_t - the charge emitted from the defect, q_0 - the elementary charge, A - the electrode area of the diode, d - the thickness of the depleted region and $I_{TSC}(T)$ - the measured thermally stimulated current.

3. Results and discussion

3.1. Electrical characterization and applicability of the DLTS method to LGADs

The LGADs and PIN diodes were electrically characterized by C–V and I–V measurements before and after irradiation. The I–V measurements showed an increase in the leakage current after irradiation, while the current related damage factor α of 9.6×10^{-19} A/cm, extracted from I–V curves at −20 °C, agrees well with values given in the literature [15]. Furthermore, after irradiation a shift of the breakdown voltage to higher values was observed, that however decreased when lowering the measurement temperature. C–V measurements on LGADs were performed in the temperature range of -20 °C to +20 °C with frequencies varying from 100 Hz to 1 MHz. After irradiation the C–V curves on LGADs have shown a decrease of both the capacitance and the depletion voltage of the gain layer (V_{GL}) indicating the degradation of the gain layer due to the deactivation of active boron dopants. The
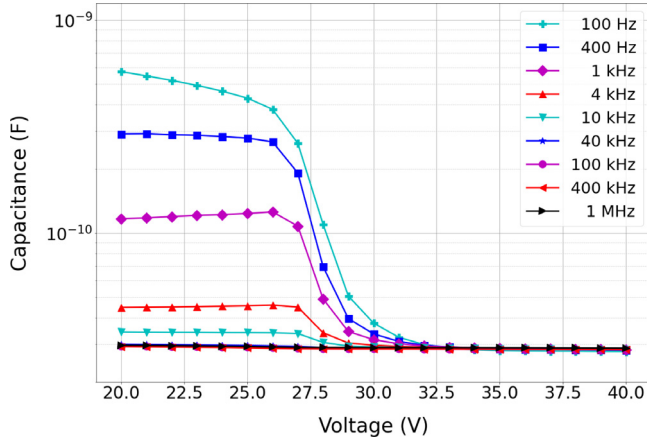
Fig. 1. *C–V measurements performed on a CNM LGAD, neutron irradiated with* 1×10^{14} n$_{eq}$/cm^2. *The measurements were performed at a temperature of -20 °C at different frequencies from 100 Hz up to 1 MHz.*
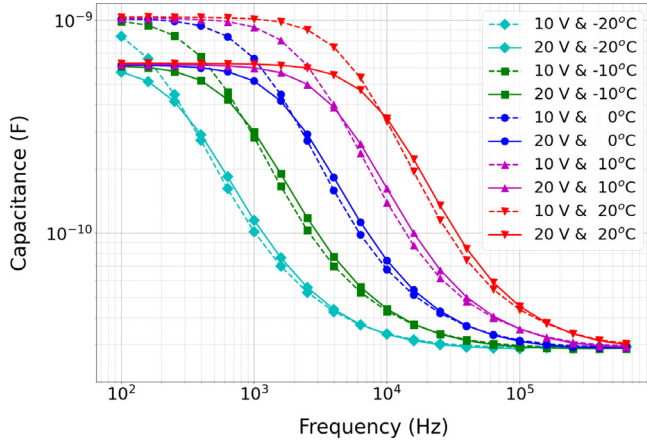

Fig. 2. Capacitance measured at certain bias voltages and temperatures in dependency of the frequency. The measurement were performed on a CNM LGAD neutron irradiated with 1×10^{14} n$_{eq}$/cm^2.

Fig. 3. DLTS spectra of EPI silicon pad diodes. The resistivity of the diodes vary due to the different boron content from 10 Ωcm to 1 kΩcm. The spectra on the left side were obtained when injecting majority carriers during the pulse step, while the spectra on the right side were recorded after majority and minority carrier injection.

V_{GL} of the investigated LGADs as well as the depletion voltage of the corresponding PIN diodes are given in Table 1. Within an error of about 4 % the same V_{GL} value was extracted for all measured ranges of temperatures and frequencies. Fig. 1 shows *C–V* measurements performed with different frequencies on a neutron irradiated CNM LGAD ($\Phi_{\mathrm{eq}} = 1 \times 10^{14}$ n$_{eq}$/cm^2). The depletion of both, the gain layer up to its depletion voltage (V_{GL}) and of the bulk region up to V_{depl}, can be well distinguished in the C-V measurements performed with low frequencies (standard: 10 kHz). For high frequencies the measured capacitance of the gain layer region significantly drops. This effect becomes even more pronounced when decreasing the temperature as shown in Fig. 2. Here the capacitance values at a certain bias below V_{GL} are plotted against the measurement frequencies. The data are taken in the temperature range of −20 °C to +20 °C.

In DLTS measurements, temperatures down to 20 K were applied and a measurement frequency of 1 MHz was used. For the standard silicon pad diodes irradiated to adequate low fluence DLTS allows very accurate measurements of radiation induced defects, as shown in Fig. 3. More details about the recorded spectra will be given below. On the other hand, DLTS measurements on LGADs resulted in non-reliable spectra due to the strong capacitance drop at high frequencies. Also the highly irradiated PIN diodes could not be measured with DLTS since in these high resistivity diodes the net background doping level is small compared to the high defect concentrations induced by irradiation.
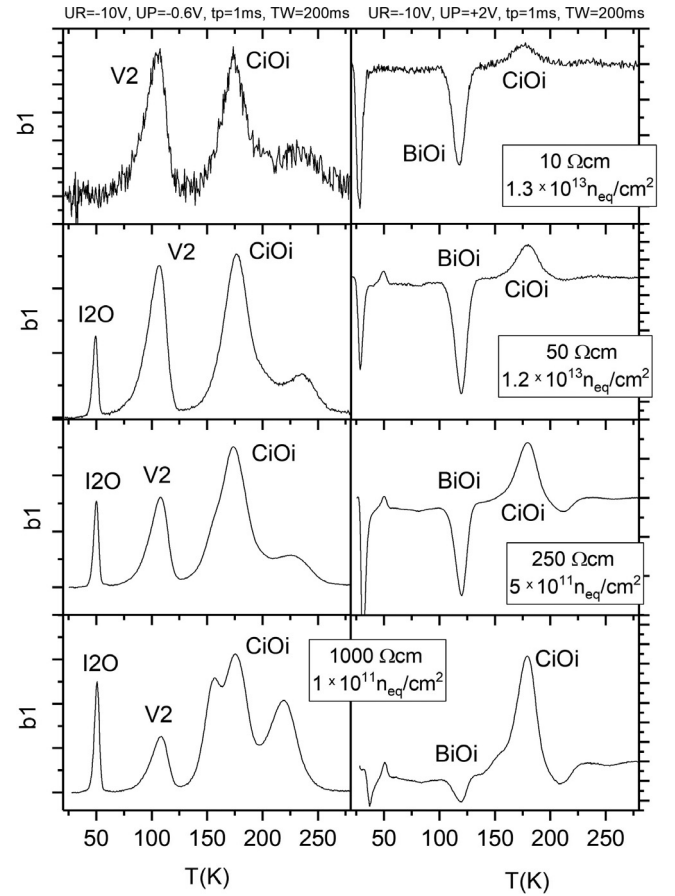
This leads to non-exponential capacitance transients during the thermal emission process and prevents reliable DLTS results [16,17].

The DLTS spectra in Fig. 3 are measured on EPI silicon pad diodes of various resistivities, from 10 Ωcm to 1 kΩcm. The 1 MeV neutron fluences are 1.3×10^{13} and 1.2×10^{13} n$_{eq}$/cm^2 for the lower resistivity samples, and 1×10^{11} and 5×10^{11} n$_{eq}$/cm^2 for the diodes with higher resistivity. On the left-hand side, spectra obtained after injection of only majority carriers (holes) are shown while on the right-hand side the spectra after minority and majority carrier injection are plotted. On the latter, as major electron trap the peak attributed to the B$_i$O$_i$ defect is observed. Analysis of the capacitance transients gave the defect concentrations from which we extracted the B$_i$O$_i$ defect introduction rates. They are plotted in Fig. 4 vs. particle fluence Φ_{eq} (white shaded area). The full symbols in this figure correspond to values taken from 1 MeV neutron irradiated diodes, while the open symbols and the half-open symbols are taken from comparable studies performed on 200 MeV electron irradiated diodes and 23 GeV as well as 230 MeV proton irradiated EPI silicon pad diodes, respectively. As it can be observed in Fig. 4, in the lower fluence range where DLTS is applicable the IRs show rather a dependence on the device resistivity than on the fluence. Thus, for high resistivity material the IRs are below 0.2 cm^{-1}, medium resistivity samples show IRs in the range of 0.6 to 0.8 cm^{-1}, and for silicon pad diodes with low resistivities the values are above 0.8 cm^{-1} and in good agreement with previous experimental results on EPI silicon pad diodes [18,19] as well as with the defect kinetic model described in the introduction [8]. Furthermore, in this fluence range for which the DLTS technique can be applied no clear dependence of the IR on the particle type can be stated. However, a dependency of the
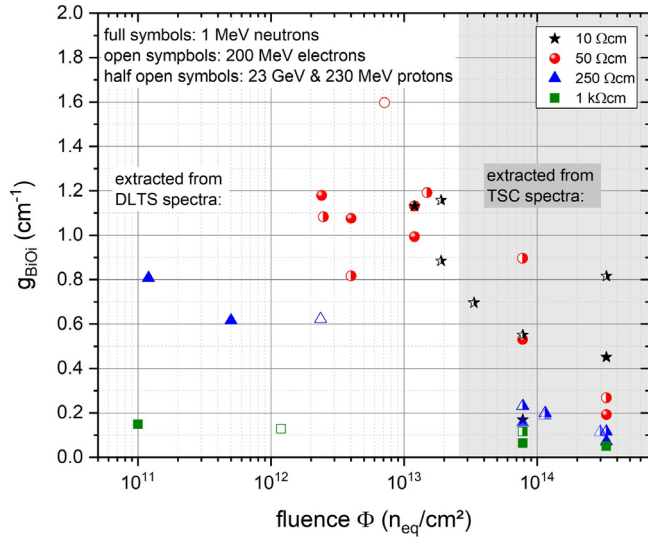
Fig. 4. B_iO_i introduction rates as function of 1 MeV neutron equivalent fluence. The values below 3×10^{13} n_{eq}/cm^2 were calculated from B_iO_i defect concentrations obtained from DLTS measurements on neutron (full symbols), electron (open symbols) and proton (half open symbols) irradiated EPI silicon pad diodes of different resistivity. For fluences above 3×10^{13} n_{eq}/cm^2 the data were extracted from the B_iO_i peak measured by TSC (grey shaded area).

IR on the particle type becomes visible at higher fluences, where the IR for proton irradiated sensors (half open symbols) are always higher than those for the neutron irradiated ones with the same resistivity (full symbols). This effect can be understood by a higher point defect formation ratio of protons compared to neutrons which preferentially create more cluster like defects [10]. A more detailed discussion about the IRs obtained by TSC (grey shaded area in Fig. 4) will be given in the next section.

3.2. TSC studies on silicon pad diodes and LGADs

Defect spectroscopy studies, including DLTS and TSC in combination with e.g. Electron Paramagnetic Resonance (EPR), Infra-Red absorption spectroscopy (IR) and detailed annealing studies, on a broad variety of irradiated silicon pad diodes have enabled the identification and assignment of a whole set of radiation induced defects in silicon [10,20–30]. Fig. 5 (top) shows TSC spectra measured on silicon pad diodes with resistivities of 250 Ωcm and 1 kΩcm, after 1 MeV neutron irradiation with fluences of 7.8×10^{13} n_{eq}/cm^2 and 3.3×10^{14} n_{eq}/cm^2, respectively. The spectra are normalized to the B_iO_i peak height and those corresponding to the highest irradiation fluence are shifted on the *y*-axis for a better visibility. Besides point defects like E(30), H(40), I_2O, VO_i, B_iO_i and C_iO_i, also multi-vacancy and cluster related defects (e.g. H(116), H(140), H(153)) [25,26] can be distinguished at temperatures above 100 K. Since the free carrier capture cross section of the C_iO_i is strongly temperature dependent, it becomes visible in TSC only at higher T_{fill} (see e.g. bold grey line in Fig. 5 with $T_{fill} = 70$ K). In the temperature range of 96 K – 98 K we can identify the peak maximum of the B_iO_i defect, that is assumed to be the main responsible defect for the radiation induced ARE.

By fitting the TSC peak area and applying Eq. (1) we extracted the B_iO_i defect concentration and the corresponding IR. The values are plotted in the grey shaded area of Fig. 4. All the IRs for the B_iO_i defect obtained by TSC for the diodes irradiated with hadrons are below the values extracted from DLTS after lower irradiation. It should be mentioned that for the highly doped diodes (10 and 50 Ωcm) an underestimation of the defect concentration has to be considered since those sensors could not be fully depleted during the TSC temperature scan. Therefore, at least for these sensors the IR should be higher than
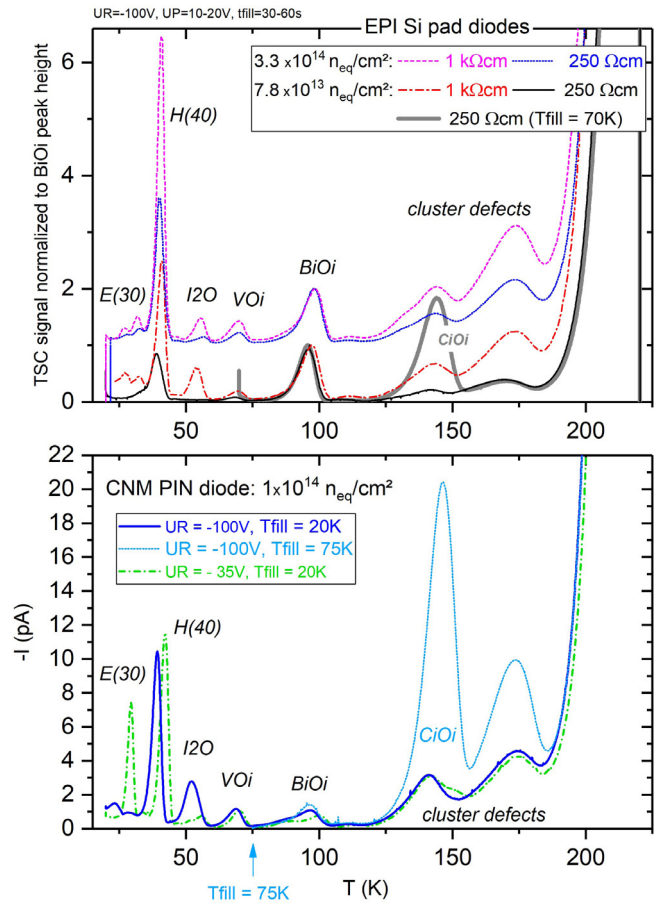

Fig. 5. (Top) TSC spectra of neutron irradiated EPI silicon pad diodes. The spectra are normalized to the B_iO_i peak height and those with higher irradiation are shifted on the y-scale. The grey spectrum (bold solid line) was taken on a 250 Ωcm diode irradiated to 7.8×10^{13} n_{eq}/cm^2 and illustrates the filling temperature dependence of the C_iO_i peak ($T_{fill} = 70$ K). (Bottom) TSC spectra of a neutron irradiated CNM PIN diode. The spectra differ in the applied reverse bias. The light blue spectra (dotted line) was taken at UR = −100 V and $T_{fill} = 75$ K.

depicted in Fig. 4. The lower doped sensors (250 and 1 kΩcm) can be fully depleted and show the same trend of decreasing of the IR with increasing the irradiation fluence.

When comparing the types of defects created in the EPI silicon pad diodes (Fig. 5 (top)) with those created in the CNM PIN irradiated with 1×10^{14} n_{eq}/cm^2 (Fig. 5 (bottom)) it is found that they are very similar. By increasing the filling temperature, also for the CNM PIN diode the C_iO_i peak becomes visible. The peak close to 100 K can be assigned to the B_iO_i defect with a concentration of about 1.5×10^{12} cm^{-3}. As a reminder, the resistivity of the CNM PIN diode is below 5 kΩcm, resulting in an effective doping level of about 2.6×10^{12} cm^{-3}. The B_iO_i IR would be around 0.02 cm^{-1}. Here we should mention that the B_iO_i peak shows a shoulder at the low temperature side whose origin is not fully clear yet, but could be connected to the so-called X-defect presented in the literature [19].

When changing the applied reverse bias (from −100 V to −35 V) the influence of the electrical field to the carrier emission becomes visible, and affects especially the TSC peaks at low temperatures, corresponding to defect levels near to the band gap edges ($E_{C,V}$). This so-called Poole–Frenkel effect is explained by an enhanced emission probability from Coulombic traps due to a field induced lowering of the emission barrier height for trapped charges [25,31,32]. It leads to a shift of the corresponding TSC peak to lower temperatures with increasing bias, and gives an explanation why for example the E(30) which is an electron trap with an energy level in the upper part of the band gap that
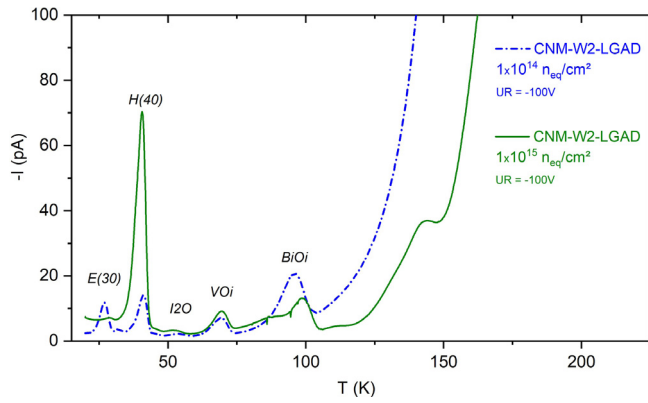
Fig. 6. TSC spectra of LGADs neutron irradiated at different fluences. The TSC spectra were recorded while applying a reverse bias of $-100\,\text{V}$.
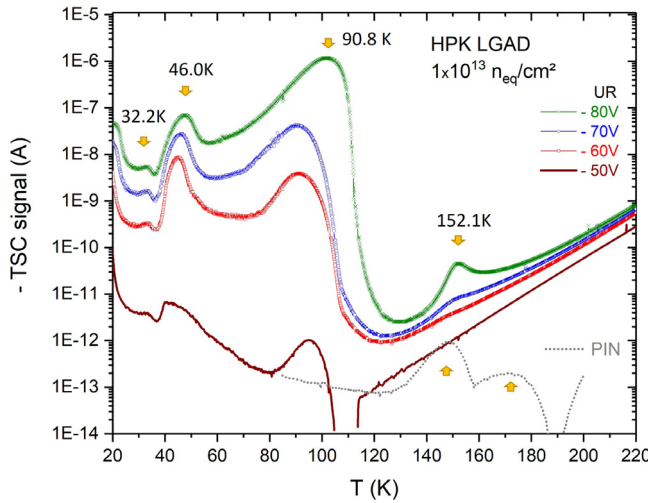

Fig. 7. TSC spectra taken at different reverse bias of an LGAD irradiated with $1\times10^{13}\,\text{n}_{eq}/\text{cm}^2$ neutrons. The dotted grey line is the TSC spectrum of the corresponding PIN diode irradiated at the same fluence.

Fig. 8. TSC spectra of a CNM LGAD irradiated with $1\times10^{14}\,\text{n}_{eq}/\text{cm}^2$ neutrons. The reverse bias voltage was varied in the range of $-10\,\text{V}$ up to $-100\,\text{V}$. The inset shows a zoom of the spectra between $50\,\text{K}$ and $125\,\text{K}$.

shows a strong Poole–Frenkel effects [26] becomes visible only for low applied bias.

Fig. 6 shows TSC spectra measured on CNM LGADs irradiated at different fluences (blue dash-dotted line: $1\times10^{14}\,\text{n}_{eq}/\text{cm}^2$ and green solid line: $1\times10^{15}\,\text{n}_{eq}/\text{cm}^2$). The reverse bias applied during the measurement was in both cases $U_R = -100\,\text{V}$, leading to full depletion of the devices (gain layer and low doped bulk). From these spectra we could identify the same defect types as measured in the PIN diode, however the peak heights are higher in the spectra of the LGAD devices. Thus, the B_iO_i concentration for the $1\times10^{14}\,\text{n}_{eq}/\text{cm}^2$ neutron irradiated LGAD is about $2\times10^{13}\,\text{cm}^{-3}$ resulting in an IR of about $0.2\,\text{cm}^{-1}$. This IR value is higher than the one of the PIN diodes but does not reach the value expected from the macroscopic sensor degradation given in the literature for highly doped LGAD gain layers [8]. Therefore, it is not very likely that this value reflects the deactivation of boron in the LGAD gain layer. Furthermore, it is observed that the increase of the background leakage current, contributing to the TSC signal, starts at temperatures significantly lower compared to the PIN or silicon pad diodes. This increased current signal is an effect of the charge amplification in the gain layer of the LGADs. Therefore, in the higher irradiated LGAD, where the gain is expected to be more reduced due to the radiation induced acceptor removal, the impact of the background leakage current starts at higher temperatures than for the lower irradiated device.

The influence of the current amplification on the TSC signal becomes even more pronounced for the measurements performed on the
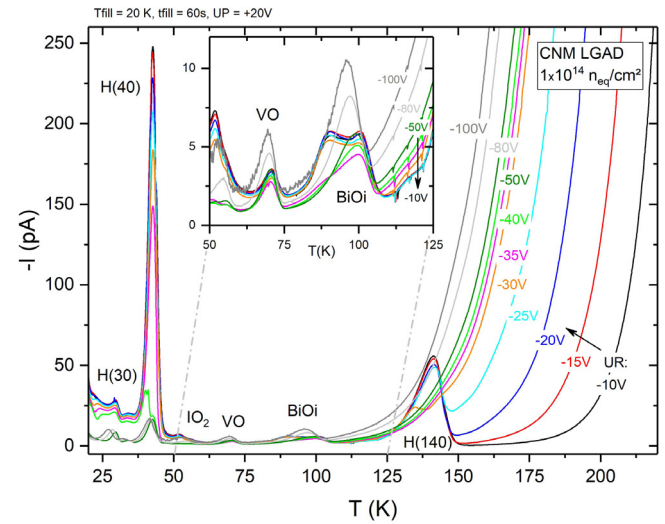
$1\times10^{13}\,\text{n}_{eq}/\text{cm}^2$ irradiated HPK LGAD (see Fig. 7). When applying a reverse bias of $U_R = -80\,\text{V}$ which corresponds to a full depletion of the device, the current signal induced by charge emission from defect states reaches values of up to $1\times10^{-6}\,\text{A}$. This would correspond to defect concentrations in the range of $10^{19}\,\text{cm}^{-3}$. The doping level of the LGAD gain layer is about $10^{16}\,\text{cm}^{-3}$, therefore the measured high current signal is an effect of the charge amplification in the gain layer and does not reflect the actual B_iO_i defect concentration. Additionally, it has to be taken into account, that for devices with multiplication layer the break-down voltage decreases with lowering the temperature [33]. For a non-irradiated HPK2-W36 LGAD it is around -50 V below 120 K compared to approximately -220 V at room temperature. In consequence it means that an exact determination of defect concentrations from the measured TSC spectra cannot be achieved unless the exact impact of the gain on the emitted charges at the given temperatures and applied voltage is known.

In a next step we checked if it is possible to distinguish between defects created in the gain layer and defects created in the low doped bulk of the devices by restricting the depletion region to the width of the gain layer region. To do so the reverse bias applied during the TSC measurements was reduced. This allows to deplete only a certain part of the device, like e.g. only the gain layer region. Therefore, the emitted charges during the heating up step are supposed to be released mainly from defects within those depleted parts. For the lower irradiated HPK LGAD the changes in the TSC signal with decreasing reverse bias are shown in Fig. 7. Up to the full depletion voltage of the gain layer ($-50\,\text{V}$), the defect related TSC current signal decreases continuously with decreasing voltage and is no longer detectable for biases below the gain layer depletion voltage. Therefore, for the low irradiated HPK LGAD it is not possible to give a reliable explanation whether the charges multiplied at higher bias voltages are coming from the bulk or gain layer region.

Comparable measurements performed on a higher irradiated CNM LGAD are illustrated in Fig. 8. First of all, one observes that with decreasing the bias voltage the background leakage current in the temperature region higher than 100 K decreases. The I–V dependence for three different temperatures (165 K, 175 K and 190 K), as extracted during the TSC scan, is plotted in Fig. 9. The red dot corresponds to the TSC current signal at 190 K and $-100\,\text{V}$ bias for the corresponding PIN diode. Additionally added are also I–V measurements of the LGAD directly performed at 190 K from low to high bias voltage. They were recorded with different waiting times between two measurement points
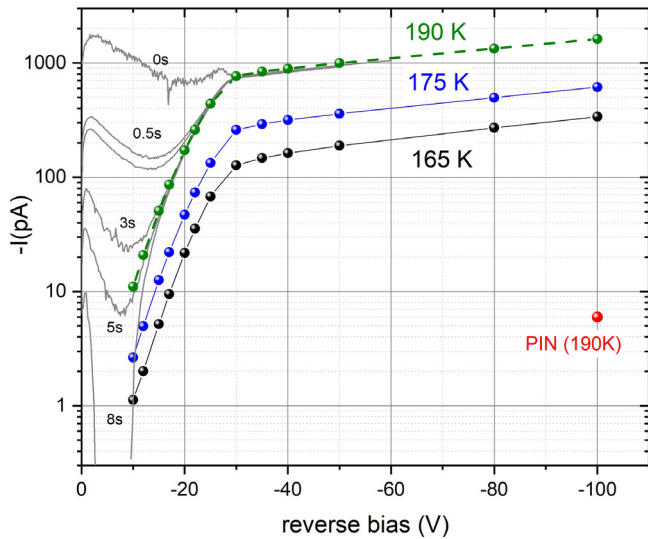
Fig. 9. TSC current values extracted from the measurements plotted in Fig. 8 at three different temperatures in dependency of the bias applied during the TSC measurement. Additionally added (solid grey lines): I–V measurements on the same LGAD performed at 190 K using different waiting times between two measurement points. Red dot labelled with PIN(190 K): From TSC measurements extracted value of the corresponding PIN.

Fig. 10. TSC spectra of a CNM LGAD irradiated with 1×10^{14} n_{eq}/cm^2 neutrons. The spectra were measured using a "voltage step" (see corresponding description in the text) and applying different reverse bias during the "heating up" step.

(≤ 10 s). The longer the waiting time, the better is the agreement of the I–V curve with the extracted values from TSC. The observed behaviour can be explained by taking into account the contribution of a time dependent displacement current at low bias. Even a sign inversion of the current signal for waiting times up to 8 s is visible leading to a minimum current value of -5.7 pA. For waiting times higher than 8 s no further changes in the measured I–V curves were observed. In summary, the I–V measurements reflect the behaviour observed during the TSC measurements and clearly demonstrate that at high voltages in the temperature range higher than 100 K the TSC signal is dominated by a high background leakage current. Therefore, when lowering the voltages during the TSC scan defect levels like the H(140) becomes visible (see Fig. 8). But also the TSC current intensities of the peaks at lower emission temperatures are influenced by the applied voltages. Especially the defect levels detected below 50 K strongly decrease in intensity when going from low to high voltages.

The inset in Fig. 8 shows a zoom of the TSC spectra between 50 K and 125 K. Normally the B_iO_i peak is expected to be measured at temperatures close to 100 K. While for low voltages this peak consists of two maxima, at higher voltages they merge into one peak. A double peak structure in this temperature range was also observed for the low doped PIN diodes and might be induced by the appearance of the X-defect [19].

Additionally to the current sign inversion that was visible in the I–V measurements at low temperatures for low applied bias, also in TSC under certain measurement conditions an inversion in the TSC signal current was observed. This is illustrated in Fig. 10. The TSC spectra here were recorded after cooling down with -100 V reverse bias (TSC procedure: step 1), making a standard filling pulse (step 2) and after the filling pulse the reverse bias was set back to $U_{step} = -100$ V (in the following called "voltage step") before applying the reverse bias UR_{up} for ramping up the temperature (step 3). As seen in Fig. 10, if after the "high voltage step" the reverse bias for ramping up is chosen to be smaller than the gain layer depletion voltage (-10 V to -25 V), the current induced by the emitted charges from defect states has a positive sign. With increasing the bias voltage up to the gain layer depletion voltage the detected emission current decreases and increases again with opposite sign for bias higher than the gain layer depletion voltage (-30 V to -150 V). The observed shifts in the defect peak maxima can
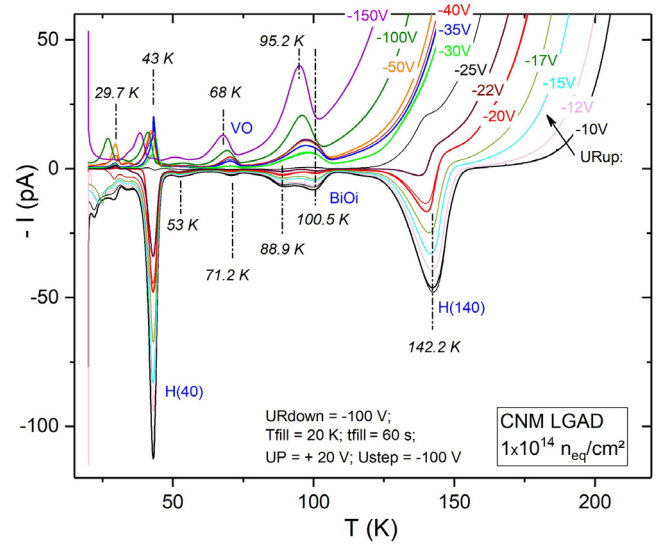
by understood by the Poole–Frenkel effect. The same behaviour is also observed for the lower irradiated HPK LGADs (not shown) and appears independent of the bias voltage applied during the TSC cooling down step. The high voltage step after the trap filling leads to a full depletion of the device. Putting afterwards the bias back to lower values most probably creates internal electric fields that counteract to the external applied field, leading charge carriers moving opposite to the external applied field. From literature it is known, that changes in the TSC current sign can appear due to internal residual electrical fields that are induced by high defect concentrations [34–36].

4. Summary

In this paper we present defect spectroscopy measurements (DLTS and TSC) on neutron, electron and proton irradiated p-type silicon pad diodes and LGADs in order to understand the feasibility of using these methods to characterize defects in LGAD structures and find indications why the acceptor deactivation in the LGAD gain layer does not correlate with the defect kinetic model which is nicely applicable for the lower doped silicon pad diodes. We demonstrate that the measured gain layer capacitance has a strong frequency and temperature dependence, resulting in a capacitance drop during DLTS measurements that makes this method not reliable for defect characterization of LGADs. In contrast, with the TSC technique defects formed in the LGAD devices can be nicely detected and compared to defects formed in irradiated silicon pad diodes. However, giving quantitative values for the defect concentrations, and therefore exact introduction rates for the boron deactivation, is challenging since the peak amplitudes are determined by the multiplication effect of the gain layer which varies with temperature and bias applied and makes it in addition difficult to clearly distinguish between defect signals coming from the low doped Si bulk or from the highly doped Si gain layer. In conclusion, based on the experimental results it can be stated that the defect spectroscopy methods we used are limited in characterizing defects in LGAD gain layers. In order to use the full potential of these methods it is therefore planned in a next step to process and characterize highly-irradiated silicon pad diodes with doping concentrations that mimic the gain layer of an LGAD.

CRediT authorship contribution statement

Anja Himmerlich: Conceptualization, Investigation, Formal analysis, Validation, Writing – original draft. **Nuria Castello-Mor:** Software, Formal analysis. **Esteban Currás Rivera:** Investigation, Formal analysis, Writing – review & editing. **Yana Gurimskaya:** Investigation, Formal analysis, Validation, Writing – review & editing. **Vendula Maulerova-Subert:** Software. **Michael Moll:** Conceptualization, Writing – review & editing, Supervision, Project administration, Funding acquisition. **Ioana Pintilie:** Validation, Conceptualization, Writing – review & editing, Project administration, Funding acquisition. **Eckhart Fretwurst:** Conceptualization, Writing – review & editing, Project administration, Funding acquisition. **Chuan Liao:** Validation, Writing – review & editing. **Jörn Schwandt:** Conceptualization, Writing – review & editing, Project administration, Funding acquisition.

Declaration of competing interest

The authors declare that they have no known competing financial interests or personal relationships that could have appeared to influence the work reported in this paper.

Data availability

Data will be made available on request.

Acknowledgements

References

[1] ATLAS Collaboration, Technical Proposal: A High-Granularity Timing Detector for the ATLAS Phase-II Upgrade, CERN-LHCC-2018-023. LHCC-P-012, CERN, Geneva, 2018, https://cds.cern.ch/record/2623663.

[2] CMS Collaboration, Technical Proposal for a MIP Timing Detector in the CMS Experiment Phase 2 Upgrade, CERN-LHCC-2017-027. LHCC-P-009, CERN, Geneva, 2017, https://cds.cern.ch/record/2296612.

[3] G. Kramberger, M. Baselga, V. Cindro, P. Fernández-Martínez, D. Flores, Z. Galloway, A. Gorisek, V. Greco, S. Hidalgo, V. Fadeyev, I. Mandić, M. Mikuz, D. Quirion, G. Pellegrini, H.-W. Sadrozinski, A. Studen, M. Zavrtanik, Radiation effects in Low Gain Avalanche Detectors after hadron irradiations, J. Instrum. 10 (2015) P07006, http://dx.doi.org/10.1088/1748-0221/10/07/P07006.

[4] M. Ferrero, R. Arcidiacono, M. Barozzi, M. Boscardin, N. Cartiglia, G.D. Betta, Z. Galloway, M. Mandurrino, S. Mazza, G. Paternoster, F. Ficorella, L. Pancheri, H.-F.W. Sadrozinski, F. Siviero, V. Sola, A. Staiano, A. Seiden, M. Tornago, Y. Zhao, Radiation resistant LGAD design, Nucl. Instrum. Methods Phys. Res. A 919 (2019) 16–26, http://dx.doi.org/10.1016/j.nima.2018.11.121.

[5] G.D. Watkins, Intrinsic defects in silicon, Mater. Sci. Semicond. Process. 3 (4) (2000) 227–235, http://dx.doi.org/10.1016/S1369-8001(00)00037-8.

[6] R. Jones, A. Carvalho, J. Goss, P. Briddon, The self-interstitial in silicon and germanium, Mater. Sci. Eng. B 159–160 (2009) 112–116, http://dx.doi.org/10.1016/j.mseb.2008.09.013, EMRS 2008 Spring Conference Symposium K: Advanced Silicon Materials Research for Electronic and Photovoltaic Applications.

[7] L.C. Kimerling, M. Asom, J. Benton, P. Drevinsky, C. Caefer, Interstitial Defect Reactions in Silicon, in: Defects in Semiconductors 15, in: Materials Science Forum, vol. 38, Trans Tech Publications Ltd, 1989, pp. 141–150, http://dx.doi.org/10.4028/www.scientific.net/MSF.38-41.141.

[8] M. Moll, Acceptor removal - Displacement damage effects involving the shallow acceptor doping of p-type silicon devices, PoS Vertex2019 (2020) 027. 12 p, http://dx.doi.org/10.22323/1.373.0027.

[9] K. Lauer, K. Peh, S. Krischok, S. Reiß, E. Hiller, T. Ortlepp, Development of Low-Gain Avalanche Detectors in the frame of the acceptor removal phenomenon, Phys. Status Solidi (A) (2020) 2200177, http://dx.doi.org/10.1002/pssa.202200177.

[10] Y. Gurimskaya, P. Dias de Almeida, M. Fernandez Garcia, I. Mateu Suau, M. Moll, E. Fretwurst, L. Makarenko, I. Pintilie, Radiation damage in p-type EPI silicon pad diodes irradiated with protons and neutrons, Nucl. Instrum. Methods Phys. Res. A 958 (2020) 162221, http://dx.doi.org/10.1016/j.nima.2019.05.062.

[11] J. Stefan Institute, https://www.ijs.si/ijsw/V001/JSI, (accessed on October 25th, 2022).

[12] CERN, The Proton Synchrotron, https://home.cern/science/accelerators/proton-synchrotron, (accessed on October 25th, 2022).

[13] CLEAR, CERN Linear Electron Accelerator for Research, https://clear.cern/, (accessed on October 25th, 2022).

[14] PhysTech, Developement and Distribution of Physical Measurement Systems, http://www.phystech.de, (accessed on October 25th, 2022).

[15] M. Moll, Radiation Damage in Silicon Particle Detectors (Ph.D. thesis), Uni Hamburg, 1999.

[16] P. Blood, J. Orton, The Electrical Characterization of Semiconductors: Majority Carriers and Electron States, Academic Press, 1992.

[17] D.V. Lang, Deep-level transient spectroscopy: A new method to characterize traps in semiconductors, J. Appl. Phys. 45 (1974) 3032, http://dx.doi.org/10.1063/1.1663719.

[18] C. Besleaga, A. Kuncser, A. Nitescu, G. Kramberger, M. Moll, I. Pintilie, Bistability of the BiOi complex and its implications on evaluating the "acceptor removal" process in p-type silicon, Nucl. Instrum. Methods Phys. Res. A 1017 (2021) 165809, http://dx.doi.org/10.1016/j.nima.2021.165809.

[19] C. Liao, E. Fretwurst, E. Garutti, J. Schwandt, M. Moll, A. Himmerlich, Y. Gurimskaya, I. Pintilie, A. Nitescu, Z. Li, L. Makarenko, The boron-oxygen (B_iO_i) defect complex induced by irradiation with 23 GeV protons in p-type epitaxial silicon diodes, IEEE Trans. Nucl. Sci. 69 (3) (2022) 576–586, http://dx.doi.org/10.1109/TNS.2022.3148030.

[20] P.M. Mooney, L.J. Cheng, M. Süli, J.D. Gerson, J.W. Corbett, Defect energy levels in boron-doped silicon irradiated with 1 MeV electrons, Phys. Rev. B 15 (1977) 3836–3843, http://dx.doi.org/10.1103/PhysRevB.15.3836.

[21] J.R. Troxell, G.D. Watkins, Interstitial boron in silicon: A negative-U system, Phys. Rev. B 22 (1980) 921–931, http://dx.doi.org/10.1103/PhysRevB.22.921.

[22] E. Fretwurst, C. Dehn, H. Feick, P. Heydarpoor, G. Lindström, M. Moll, C. Schütze, T. Schulz, Neutron induced defects in silicon detectors characterized by DLTS and TSC methods, Nucl. Instrum. Methods Phys. Res. A 377 (2) (1996) 258–264, http://dx.doi.org/10.1016/0168-9002(95)01405-5.

[23] N. Zangenberg, J.-J. Goubet, A. Nylandsted Larsen, On-line DLTS investigations of the mono- and di-vacancy in p-type silicon after low temperature electron irradiation, Nucl. Instrum. Methods Phys. Res. B 186 (1) (2002) 71–77, http://dx.doi.org/10.1016/S0168-583X(01)00876-X.

[24] I. Pintilie, M. Buda, E. Fretwurst, G. Lindström, J. Stahl, Stable radiation-induced donor generation and its influence on the radiation tolerance of silicon diodes, Nucl. Instrum. Methods Phys. Res. A 556 (1) (2006) 197–208, http://dx.doi.org/10.1016/j.nima.2005.10.013.

[25] I. Pintilie, E. Fretwurst, G. Lindström, Cluster related hole traps with enhanced-field-emission - the source for long term annealing in hadron irradiated Si diodes, Appl. Phys. Lett. 92 (2) (2008) 024101, http://dx.doi.org/10.1063/1.2832646.

[26] I. Pintilie, G. Lindstroem, A. Junkes, E. Fretwurst, Radiation-induced point- and cluster-related defects with strong impact on damage properties of silicon detectors, Nucl. Instrum. Methods Phys. Res. A 611 (1) (2009) 52–68, http://dx.doi.org/10.1016/j.nima.2009.09.065.

[27] V.P. Markevich, A.R. Peaker, B. Hamilton, S.B. Lastovskii, L.I. Murin, J. Coutinho, V.J.B. Torres, L. Dobaczewski, B.G. Svensson, Structure and electronic properties of trivacancy and trivacancy-oxygen complexes in silicon, Phys. Status Solidi A 208 (3) (2011) 568–571, http://dx.doi.org/10.1002/pssa.201000265.

[28] R. Radu, E. Fretwurst, R. Klanner, G. Lindstroem, I. Pintilie, Radiation damage in n-type silicon diodes after electron irradiation with energies between 1.5 MeV and 15 MeV, Nucl. Instrum. Methods Phys. Res. A 730 (2013) 84–90, Proceedings of the 9th International Conference on Radiation Effects on Semiconductor Materials Detectors and Devices. http://dx.doi.org/10.1016/j.nima.2013.04.080.

[29] R. Radu, I. Pintilie, L.C. Nistor, E. Fretwurst, G. Lindstroem, L.F. Makarenko, Investigation of point and extended defects in electron irradiated silicon — Dependence on the particle energy, J. Appl. Phys. 117 (16) (2015) 164503, http://dx.doi.org/10.1063/1.4918924.

[30] E.M. Donegani, E. Fretwurst, E. Garutti, R. Klanner, G. Lindstroem, I. Pintilie, R. Radu, J. Schwandt, Study of point- and cluster-defects in radiation-damaged silicon, Nucl. Instrum. Methods Phys. Res. A 898 (2018) 15–23, http://dx.doi.org/10.1016/j.nima.2018.04.051.

[31] J. Frenkel, On pre-breakdown phenomena in insulators and electronic semi-conductors, Phys. Rev. 54 (1938) 647–648, http://dx.doi.org/10.1103/PhysRev.54.647.

[32] J.L. Hartke, The Three-Dimensional Poole-Frenkel Effect, J. Appl. Phys. 39 (1968) 4871–4873, http://dx.doi.org/10.1063/1.1655871.

[33] D.J. Massey, J.P.R. David, G.J. Rees, Temperature dependence of impact ionization in submicrometer silicon devices, IEEE Trans. Electron. Dev. 53 (9) (2006) 2328, http://dx.doi.org/10.1109/TED.2006.881010.

[34] I. Pintilie, C. Tivarus, T. Botila, D. Petre, L. Pintilie, Experimental evidence of deep electron and hole trapping levels in high fluence proton irradiated p–n si junctions using optical charging spectroscopy, Nucl. Instrum. Methods Phys. Res. A 439 (2) (2000) 221–227, http://dx.doi.org/10.1016/S0168-9002(99)00887-6.

[35] M. Bruzzi, R. Mori, M. Scaringella, D. Menichelli, Optimization of the priming procedure for thermally stimulated current with heavily irradiated silicon detectors, PoS RD09 (2009) 018, https://pos.sissa.it/098/018/pdf.

[36] D. Menichelli, R. Mori, M. Scaringella, M. Bruzzi, Zero-bias thermally stimulated currents (ZB-TSC) spectroscopy of deep traps in irradiated silicon particle detectors, Nucl. Instrum. Methods Phys. Res. A 612 (3) (2010) 530–533, http://dx.doi.org/10.1016/j.nima.2009.08.049.